Review Article

Imaging of nucleic acids with atomic force microscopy

Yuri L. Lyubchenko [a,*], Luda S. Shlyakhtenko [a], Toshio Ando [b]

[a] Department of Pharmaceutical Sciences, University of Nebraska Medical Center, Omaha, NE 68198-6025, USA
[b] Department of Physics, Kanazawa University, Kakuma-machi, Kanazawa 920-1192, Japan

ARTICLE INFO

ABSTRACT

Atomic force microscopy (AFM) is a key tool of nanotechnology with great importance in applications to DNA nanotechnology and to the recently emerging field of RNA nanotechnology. Advances in the methodology of AFM now enable reliable and reproducible imaging of DNA of various structures, topologies, and DNA and RNA nanostructures. These advances are reviewed here with emphasis on methods utilizing modification of mica to prepare the surfaces enabling reliable and reproducible imaging of DNA and RNA nanostructures. Since the AFM technology for DNA is more mature, AFM imaging of DNA is introduced in this review to provide experience and background for the improvement of AFM imaging of RNA. Examples of imaging different structures of RNA and DNA are discussed and illustrated. Special attention is given to the potential use of AFM to image the dynamics of nucleic acids at the nanometer scale. As such, we review recent advances with the use of time-lapse AFM.

© 2011 Elsevier Inc. All rights reserved.

1. Introduction

Nucleic acid nanotechnology is a branch of nanotechnology that utilizes the ability of nucleic acids to self-assemble into complex three-dimensional (3D) structures. The field of DNA nanotechnology was established in 80's by pioneering works of N. Seeman in which he demonstrated the possibility to assemble 3D DNA structures such as a cube from DNA oligomers of the well-defined structures (reviewed in [1]). The key elements for the DNA nanotechnology are three-way and four-way DNA junctions. These are biologically important DNA structures formed during DNA replication and recombination, respectively. Unlike DNA, which exists primarily as a double helix, RNA molecules are single stranded, so the formation of branched RNA molecules is a rule rather than exception. Loops in branched RNA molecule interact with each other to form a three-dimensional biologically important RNA structure. Unraveling principles by which such structures are formed, stabilized and transit from one into another is a problem of great importance for molecular biology. In addition, understanding the self-assembly principles of RNA open the prospects for engineering of RNA molecules with defined structural properties and desired functionality. This is the area of interest of the recently emerging field of RNA nanotechnology [2–4]. Among different nanoimaging techniques atomic force microscopy (AFM) is the very attractive due to its versatility in imaging of various DNA and RNA nanostructures and the ability to directly image dynamics of the DNA and RNA nanostructures.

Immobilization of the sample is a key step in imaging biological molecules AFM. A number of sample preparation techniques were developed for reliable AFM imaging of nucleic acids based primarily on their inherent negative charge [5–13]. The surface modification methods are focused on preparing the surface to compensate for the DNA (or RNA) charge, or forming a positively charged substrate to hold the nucleic acids electrostatically. The most common substrates for deposition of biological objects are mica [5,6,8,10,12–17], gold films [18–23], and glass [24–26]. Highly oriented pyrolytic graphite (HOPG) is used as well [27–31], although its inherent high hydrophobicity complicates routine use of this substrate for AFM studies of nucleic acids due to their hydrophilic nature. The sample preparation procedure depends on the imaging type. The sections below describe various methods to prepare the AFM substrates for each type of imaging. A special emphasis is given to AFM studies of RNA nanoassembles [2]. Historically the procedures were developed for imaging of duplexes of DNA and RNA [6,14]. Later they were applied to branched DNA nanostructures (reviewed in [13,32–34]).

2. Experimental design

The sample preparation methods described below were developed for DNA, but they are fully applicable for imaging of RNA nanostructures as shown in [2,35].

---

* Corresponding author. Address: Department of Pharmaceutical Sciences, College of Pharmacy, COP 1012, University of Nebraska Medical Center, 986025 Nebraska Medical Center, Omaha, NE 68198-6025, USA. Fax: +1 402 559 9543.
E-mail address: ylyubchenko@unmc.edu (Y.L. Lyubchenko).

2.1. Mica properties and preparation as an AFM substrate

Mica is a layered mineral with potassium cations located between the hydroxyl groups of the layers [36]. The attractive feature of mica as a substrate for AFM studies is the smoothness of the surface. Mica, primarily muscovite mica, is the most widely used substrate for AFM imaging of various biological objects, nucleic acids in particular. All commercially available mica sheets (green or ruby mica) Asheville-Schoonmaker Mica Co. (Newport News, VA) are thick and large (more than 5×7 cm) sheets suitable for making substrates of different sizes.

Mica when cleaved along the layers using either razor blades or Scotch tape is ready for use. Freshly cleaved mica is an atomically flat surface several microns thick. After cleavage along the layers, potassium cations are distributed on both sides, leaving an uncompensated negative charge on both surfaces of mica. Thus, freshly cleaved negatively charged mica is a perfect AFM substrate for positively charged molecules. The adsorption of negatively charged molecules, such as nucleic acids, requires special surface and/or sample preparation procedures. These procedures can be divided into two classes: treatment of mica with divalent cations [37–42] and chemical modification of mica [42–48]. In a few applications, mica is coated with polylysine and cationic lipids; the protocols can be found in [43] and [11], respectively. The sections below describe the procedures for the two major methods.

2.2. Treatment of mica with divalent cations

Initially, Brack [44] suggested the pretreatment of mica with Mg^{2+} cations to prepare the sample for transmission electron microscopy. This idea was eventually implemented into the procedure for preparing the mica surface for DNA imaging [5,8].

2.2.1. Overview of the cation-assisted procedure

In this approach, mica is incubated in a solution containing 5–10 mM Mg^{2+}, where the resulting substrate holds DNA molecules onto the surface, enabling reliable imaging with AFM. Later experiments have shown that pretreatment of mica with cations is not necessary, but Mg^{2+} cations should be present in the deposition buffer [5,8,10,16,45–47]. Also, later studies extended the repertoire of metal cations, so that divalent cations such as Ni^{2+}, Mg^{2+}, Co^{2+} or Zn^{2+} could be used to hold the DNA molecules on the surface for imaging with AFM [37,40], and the addition of a monovalent salt to the deposition buffer would release the DNA molecules from the surface [48]. The optimum cation concentration is ∼1 mM, with no DNA bound at 0.1 mM and ∼50% of the maximal DNA binding at 10 mM. The DNA binding efficiency depends not only on the concentrations of the metal cations, but also on their radii [37]. When the ionic radius is 0.74 Å or less, DNA binds tightly to the mica and can be imaged with AFM directly in solution. Increasing the ionic radii of the cations weakens the DNA binding. Despite the wide use of the technique (e.g., [10,12,16,37,40,45–47]), the mechanism of DNA adsorption onto a mica surface in the presence of divalent cations is not entirely clear [48–51]. The counterions decrease the electrostatic repulsion between the DNA and mica surface and may also function as bridges that keep the negatively charged DNA near the mica surface. The distribution and balance of counterions near each of these surfaces are also driving forces of the adsorption process [48–52].

The application of this procedure for imaging of the RNA nanostructures is described in Section 3.3.

2.2.2. Methodology for the cation-assisted procedure

The protocol for the sample preparation is straightforward. Below is the protocol provided in [37] in which various DNA samples were imaged with AFM:

(1) Cleave mica immediately before use.
(2) Prepare DNA solution 1–20 ng/μL (depends on the DNA type and the length) in buffer containing 40 mM HEPES buffer (pH 7.0) and 10 mM MgCl$_2$.
(3) Place 1 μL of the DNA solution on the mica surface, incubate for 1–3 min, and rinse with 2–4 mL of deionized water.
(4) Dry the specimens under compressed air and further dry in a desiccator over P$_2$O$_5$. Image with the Tapping mode AFM method.

2.2.3. Major features of the cation-assisted procedure and potential pitfalls

The simplicity of the preparation of the DNA sample is the most attractive feature of cation-assisted technique. The surface remains smooth, enabling high-resolution AFM studies. At the same time, a number of issues with this method need to be taken into consideration. The major one is the change of DNA structure and morphology by divalent cations. For example, Zn^{2+} induces DNA kinking [53,54]. DNA remains kinked in mixed Mg^{2+}/Zn^{2+} electrolytes until the Zn^{2+} concentration is reduced below 100 μM. Replacing one type of cation with another usually alleviates the problem. Mg^{2+} cations are used preferentially, although for imaging protein–DNA complexes, Ni^{2+} cations are often used. Regardless of the divalent cation used for the deposition, DNA appears stiffer in the images than it should be in solution with the persistence length larger than in solution [61–67]. In addition, sequence can affect the flexibility of the DNA. This effect should be taken into account if the DNA bending is analyzed at scales below 100 nm [55]. Finally, cation-assisted techniques complicate AFM imaging of supercoiled DNA. These are circular DNA molecules with plectonemic geometry due to uncompensated overall twist. The overall geometry of supercoiled DNA is rather labile and sensitive to environmental conditions. In initial AFM experiments, with the use of the Mg-assisted approach [5,8], supercoiled DNA molecules appeared on the images as fully relaxed circular molecules. Further development of the Mg-assisted method made it possible to visualize plectonemic superhelices, but the sizes of the supercoiled loops widely varied. In addition, large loops and tightly twisted segments of the plectonemic superhelix appeared between the loops (reviewed in [56]). Such DNA morphology is in contrast with the images of supercoiled DNA obtained with electron microscopy, along with numerous physical chemical data and computer modeling (paper [57] and references therein). The problem was eased in later experiments in which a modified procedure was used. In these experiments, DNA was deposited onto freshly cleaved mica from the solution containing divalent cations. This methodology enabled to preserve the plectonemic morphology of supercoiled DNA molecules [58]. Thus, a number of potential problems in the procedure for DNA preparation can interfere with the quality of AFM imaging and should be taken into account.

2.3. Chemical modification of mica

Alternative approaches chemically modify mica with silanes that controllably change the surface charge to yield a positively charged mica surface [6,13,14,59]. Two major techniques are described in the sections below. Both methods are applied to AFM imaging of DNA and RNA including DNA [32,33] and RNA nanostructures [60].

2.3.1. Chemical modification of mica with APTES

Treatment of mica with 3-aminopropyltriethoxy silane (APTES), termed AP-mica, was developed simultaneously with the Mg-type methods for imaging DNA [6,14] and was applied later to various protein–DNA complexes [6,14,59,61]. The reaction of APTES is shown schematically in Fig. 1. The reaction leads to covalent
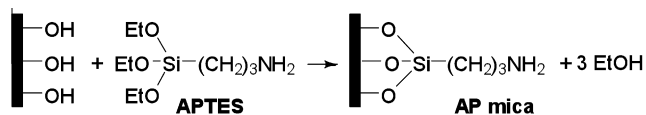
Fig. 1. Scheme of mica reaction with 3-aminopropopyltriethoxy silane (APTES).

attachment of aminopropyl groups that are positively charged due to the protonation of amino groups.

2.3.1.1. Methodology for the AP-mica procedure. The vapor deposition procedure prepares smooth mica surfaces with a roughness similar to untreated mica. The procedure has been described in detail [13]. Briefly:

- Freshly cleaved mica sheets are mounted on top of a 3L glass desiccator.
- A plastic container with 30 μL of distilled APTES is placed at the bottom of the desiccator.
- The lid is closed to allow the chemical to evaporate, yielding AP-mica in 2 h.
- The container with APTES is removed and the desiccator is filled with Ar gas.
- AP-mica retains its DNA binding activity for 2 weeks with no accumulation of visible contamination.
- The procedure produces a surface with uniform distribution of DNA molecules in no preferred orientation.

2.3.1.2. Major features of the AP-mica procedure and drawbacks.
- AP-mica remains protonated (positively charged) over a broad range of pH values up to pH 10. This important feature provides an enormous flexibility in using APTES-treated surfaces.
- The sample can be deposited on the AP-mica surface in a broad range of pH and ionic strengths, without the presence of divalent cations.
- The samples prepared on AP-mica are stable over months without any accumulation of impurities. Thus, a large number of images can be acquired without fear of sample deterioration.
- The deposition onto AP-mica preserves the plectonemic geometry of supercoiled DNA.

This last important feature of AP-mica is illustrated by Fig. 2, which shows AFM images of supercoiled DNA. The plectonemic morphology of the DNA molecules is clearly seen on all molecules in the field. Moreover, the sensitivity of the geometry of supercoiled DNA to ionic strength was tested in the AP-mica approach [15,62]. DNA binds to AP-mica primarily due to electrostatic interactions between the protonated amino groups of the AP-mica substrate and the negatively charged DNA backbone. Also note that the geometry of immobilized supercoiled DNA molecules resembles two-dimensional projections of unperturbed DNA molecules onto a plane because of the low surface charge density of AP-mica. The latter feature suggests that the AP-mica technique is appropriate for studying global DNA conformations [63].

This approach has a drawback. During time-lapse AFM imaging in aqueous solution, rather large aggregates appeared on the surface, presumably due to the hydrolysis of APTES molecules and their fast aggregation. These observations suggest that in addition to covalent binding of APTES, molecules adsorb loosely to the surface and form aggregates after hydrolysis [64].

2.3.2. Mica functionalization with 1-(3-aminopropyl)silatrane – APS-mica method

As a useful alternative to APTES, 1-(3-aminopropyl)silatrane (APS) alleviates the problems outlined above [17,32,33]. Similar to APTES, this reagent binds covalently to hydroxyl groups of silicon surfaces (Fig. 3).

2.3.2.1. Methodology for the APS-mica procedure.
- Prepare a 50 mM APS stock solution in water and store it in a refrigerator. The shelf life of the stock solution is greater than 6 months.
- Prepare a working APS solution for mica modification, dissolving the stock solution at 1:300 in water; it can be stored at room temperature for several days.
- Cleave mica sheets of needed sizes (typically 1 × 3 cm) at 0.05–0.1 mm thickness, place them in appropriate plastic tubes, pour working APS solution to cover the sheets, and leave them on the bench for 30 min.
- Remove the mica sheets, wash with deionized water and dry them under an argon stream. The strips are ready for the sample preparation. The APS mica sheets remain active for several days.

2.3.2.2. Major features of the APS-mica procedure. Unlike APTES, which is commonly used for silica surface modifications, APS is less reactive and extremely resistant to polymerization at neutral pH. A
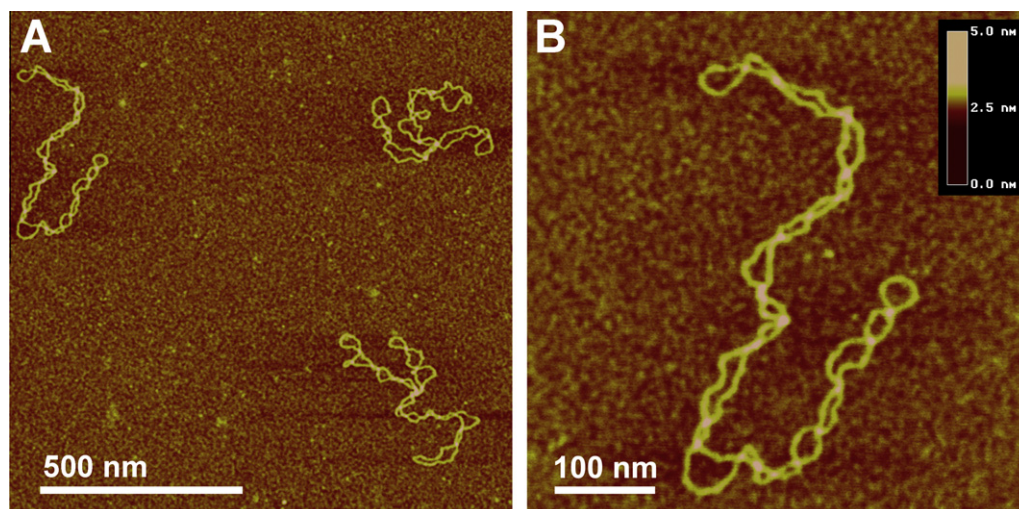
Fig. 2. AFM images of supercoiled DNA deposited onto AP-mica. After deposition onto AP-mica, the samples were rinsed with water and argon dried. The images were acquired in air with Multimode AFM (Nanoscope III, Veeco) operating in Tapping mode.
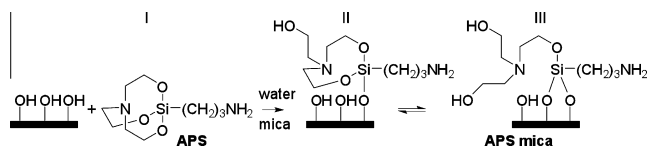
Fig. 3. Scheme of mica modification by 1-(3-aminopropyl)silatrane. APS (I) reacting with the hydroxyl groups of mica, forming a transient molecule (II), and yielding a product (III).

suggested mechanism of the surface modification is shown in Fig. 3. The final product APS-mica (III) is obtained after partial hydrolysis of the intermediate (II) on the surface. Apparently, the stabilizing triethanolamine unit remains attached to the Si atom in APS-mica, so the linkage to the surface is more easily hydrolyzed than the surface functionalized with APTES. A procedure has been developed for preparing APS-mica with characteristics similar to that of AP-mica (smoothness, stability, etc.) [17,32,33].

APS is not commercially available, but can be synthesized using standard organic chemistry lab equipment [17,32]. The preparation of APS-mica for AFM is described in detail in [32].

2.4. Other substrates for DNA immobilization

This section provides a brief overview of techniques that use substrates other than mica. A highly oriented pyrolytic graphite (HOPG) [27,28,30,31] and epitaxially grown gold films [19,22,23] can be used for AFM imaging of DNA and its complexes. Both substrates are rather inert and need additional chemical activation for adsorption of nucleic acids. Gold substrates can be modified by organic thiols or bifunctional disulfides to increase their affinity. Nucleic acids can then be covalently attached to the functionalized surface [18–23,65].

An attractive property of HOPG and gold is that they are conductive substrates and can be used for scanning tunneling microscopy (STM) studies of DNA of various sizes and nucleotide composition [66–69]. Similar to mica, HOPG has a layered structure that can be cleaved with sticky tape. However, structural defects and the fine structure in step edges of pure graphite often resemble the expected structure of DNA and thus can be misleading during DNA imaging [70–73]. Note that HOPG is a hydrophobic substrate, which complicates its use for imaging hydrophilic samples such as DNA. HOPG can be modified for binding DNA through multiple steps of chemical treatment. The final formation of thiol groups on the surface allows binding of mercurated DNA for imaging with a scanning probe microscope [74]. Recently, a simplified procedure for modifying HOPG was proposed [30]. The authors used a graphite modifier composed of a hydrocarbon–peptide pair terminating with an amine group: $(CH_2)_n$-$(NCRH_2CO)_m$-NH_2 [30,75,76]. The application of this graphite modifier to the hydrophobic HOPG surface results in the formation of a thin (0.7 nm) monolayer of positively charged polymer on the graphite surface, which promotes DNA binding. The surface is rather smooth, allowing the authors [75] to image triple-stranded poly (dG)-poly (dG)-poly (dC) molecules in addition to poly (dG)-poly (dC) duplexes. Interestingly, single-stranded regions within these polymers were detected as well.

2.5. AFM instrumentation

Additional improvements of AFM instrumentation were needed for routine use of AFM in biological studies. An intermittent contact mode (IC mode) has been an efficient modification of the instrument for AFM imaging in numerous biological applications. Initially, this mode was termed Tapping mode [77], but the name

has been trademarked by the AFM manufacturer, Veeco. Therefore, other manufacturers utilize this methodology under different names such as alternating contact (AC) mode. In the contact mode, the tip–sample distance is maintained via measuring the deflection of the tip cantilever determined by the van der Waals repulsion forces, but the detection principle for the intermediate mode is different. In AC/IC/TM-AFM, a cantilever is deliberately vibrated at a frequency close to the cantilever resonant frequency by a piezo-electric modulator with very small amplitude. As the tip approaches a surface, the van der Waals attractive force between the tip and the sample changes both the amplitude and the phase of the cantilever vibration. These changes are monitored by a Z-servo system feedback loop to control the tip–sample distance. The ability of the AC/IC/TM mode to gently image biological samples was the major attractive feature of this operating mode. Although acoustic excitation is primarily used to drive the tip oscillation, magnetically coated cantilevers can be driven with an oscillating magnetic field [53]; this useful principle is implemented in the Agilent AFM instruments. Currently, many companies manufacture AFM instruments that are quite comparable in their characteristics.

3. AFM study of branched DNA and RNA molecules

Although DNA primarily exists as a linear double helical polymer, during certain stages of the cell cycle, it adopts more complex branched configurations. For example, three-way (three-arm) junctions are the models for replicating DNA, whereas a structure with four arms linked together at a four-way junction is formed during DNA recombination. Structural characterization of such DNA structures is important for understanding the molecular mechanisms of the corresponding genetic processes. Compared to DNA, branching of RNA molecules is the rule rather than the exception. RNA molecules are primarily single stranded, but intramolecular base pairing due to complementary short regions results in the formation of hairpins. Using imaging to identify hairpin regions and their interaction with each other is important for understanding the functions of these 3D RNA structures [78]. For example, many RNAs act as "ribozymes" and their 3D structure is critical for this function. AFM imaging would be the method of choice for such an analysis. Unfortunately, progress in this area is still modest; however, the advances in AFM resolution and in sample preparation will likely spur further progress in the AFM imaging of RNA.

3.1. AFM imaging of three-way DNA junctions

Successful imaging of three-way DNA junctions was performed with AP-mica methodology [79,80]. Three-way DNA junctions were obtained by annealing two DNA strands of different lengths. One contained an extra self-homology section capable of forming hairpins in the middle. Except for this palindrome region, the rest of the sequence of the long single strand was fully complementary to the second strand. After annealing, these regions formed long duplexes with hairpins in the middle. The sample was deposited onto AP-mica, rinsed and dried as specified for the AP-mica protocol, [13] and imaged in air. AFM images for the sample with a 27 bp hairpin are shown in Fig. 4 (see paper [80] for more images and experimental details). Hairpin duplexes located in the middle of the construct are indicated with arrows in the image. The striking feature of these three-way junctions is a large variability of the angle between the arms. For example, molecule 1 has a very small interstrand angle, but molecule 2 has an angle of ~180°. Such variability in the interarm angle indicates a highly dynamic property of three-way junctions. This variability of the angle does not
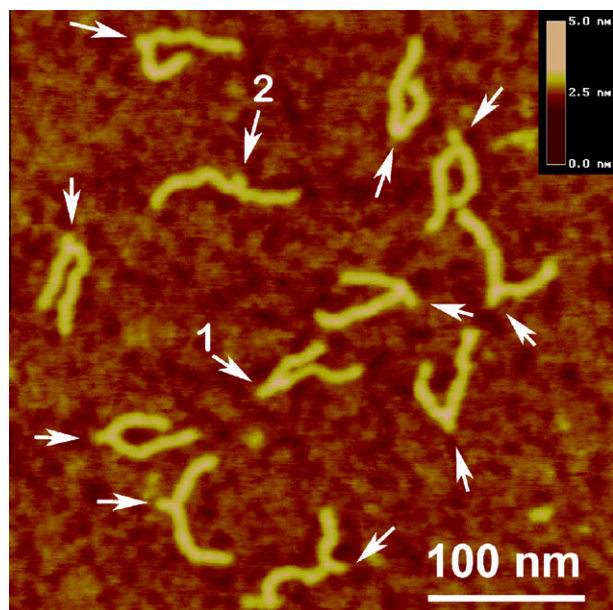
Fig. 4. AFM images of the three-way DNA junctions obtained by annealing two DNA strands with the 27 bp hairpin structure in one of the strands indicated with arrows. The images were obtained by scanning in air using Multimode AFM (Nanoscope III, Veeco) operating in Tapping mode. The figure was reprinted from publication [80]; copyright © 2000 with permission from the Oxford University Press.

Fig. 5. AFM image of dried HJs deposited onto APS-mica in Mg-containing buffer (TNM). Unambiguously classified molecules in trans (extended) and cis conformations are labeled 1 and 2, respectively. The images were obtained by scanning in air using Multimode AFM (Nanoscope III, Veeco) operating in Tapping mode. The figure was reprinted from publication [85]; copyright © 2003 with permission from the American Society for Biochemistry and Molecular Biology.

depend on the orientation of the molecule relative to the scan direction, which rules out a possible tip orientation effect. This conclusion is perfectly in line with the results obtained in solution [81,82], providing additional support for the suitability of the AP-mica procedure for analyzing dynamic 3D DNA structures.

3.2. AFM imaging of four-way DNA junctions

Four-way DNA junctions are the model system for the DNA intermediates. These structures consist of four DNA duplexes attached to each other at the ends. The biological significance of these structures is that four-way DNA junctions are formed during DNA recombination. Termed Holliday junctions (HJs) after R. Holliday who proposed the model for homologous DNA recombination [83]. Due to the enormous biological importance of HJs, various methods have been applied to characterize structure of HJs. These studies, including recent X-ray crystallography analysis, show that in the presence of multivalent cations, the junction adopts an anti-parallel orientation in which the four helices stack in pairs to form two double-helical domains (reviewed in [84]). Interestingly, the studies also revealed that enzymes only interact with folded conformations of HJs to resolve the junctions, yet these conformations do not allow branch migration to occur. Indirect data show that a fully unfolded conformation of the junction is required for branch migration [80].

AFM imaging was able to resolve this controversy in [85]. This study designed junctions capable of branch migration and used time-lapse imaging in solution to directly image the branch migration process. The molecules containing HJs were gel purified from unreacted molecules or fully migrated HJs and prepared for AFM imaging with the APS-mica methodology. Fig. 5 shows the AFM image for a sample deposited onto APS-mica and argon-dried. In the time-lapse experiments, the sample was imaged in solution. The DNA solution was injected into the fluid AFM cell and was imaged immediately after the AFM tip engaged the surface. The DNA drying step was omitted in these studies. In the continuous scanning
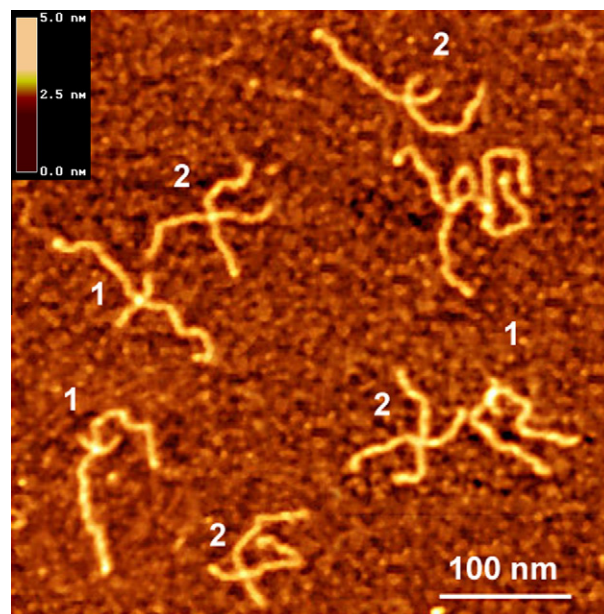
regime, the data were acquired at a rate of ~1 frame per minute. The time-lapse AFM imaging unambiguously showed that DNA conformation with parallel orientation exchanging arms (initially proposed as a model for the HJ branch migration) does not support branch migration. Unfolding of the HJs is required for branch migration. An alternative procedure using divalent cations was not applicable in these studies, as divalent cations bind strongly to the junction vertex and prevent branch migration. Thus, Mg^{2+} cations had to be removed in these experiments to start the branch migration process.

3.3. Imaging of RNA arrays

As mentioned above, unlike DNA, RNA primarily exists as a single-stranded polynucleotide, which is capable of folding into complex branched structures, depending on the sequence. Nanoimaging techniques, such as AFM, could provide important information on the tertiary structure of RNA. Another area of great interest is the use of short DNA and RNA molecules of well-designed sequence for self-assembly of nanostructures with various shapes and potential novel functions. The field was established by the pioneering works of N. Seeman [86] and is currently being applied for designing multifunctional nanostructures. We focus here on a few recent works involving application of AFM imaging to study nanoassembly of RNA molecules.

In a series of works led by Jaeger [87,88], AFM was used to demonstrate the critical importance of the loop–loop interaction (kissing loop arrangement) in the assembly of hairpin-looped RNA molecules (tecto RNAs) into square-shaped structures. The nanosquares' assembly is stabilized by Mg^{2+} cations; therefore, AFM imaging was performed in the presence of 15 mM Mg^{2+} cations and samples were prepared with the cation-assisted procedure. Note that in addition to imaging dry sample, imaging in 15 mM Mg acetate solution was used to observe the assembly process [88]. The sample was placed on the mica surface, and the formation of nanostructures via kissing-loop formation was observed by slow

cooling from 50 to 4 °C. The structures appeared on the AFM images during repetitive scanning in the buffer.

Another interesting application of the RNA-based nanodesign is a series of works by P. Guo [78,89,90]. His group found that a small viral procapsid RNA (pRNA) plays an essential role in packaging viral DNA into the procapsid of the bacteriophage phi29. The DNA-packaging motor of phi29 contains six copies of pRNA molecules that together form a hexameric ring. It binds to the connector of procapsids (the unique site on procapsids where DNA enters and exits) as the first step in DNA packaging. A loop/loop interaction of pRNA molecules forms the hexameric ring, which contains two regions: a helical region and a self-folded region, including right and left loops as described in [90]. The interactions between pRNA molecules can result in the formation of not only a hexameric ring, but also other oligomers like dimers or trimers.

The interactions of these pRNA molecules were studied with a cryo-AFM instrument (operates under cryogenic temperatures, 80–90 K), which was developed in the lab of Z. Shao [91]. The major feature of cryo-AFM is an improved resolution due to the elimination of capillary forces [91,92]. The samples of pRNA for cryo-AFM were prepared by a direct deposition of solution of RNA molecules. The samples were prepared with the use either Mg-assisted procedure and freshly cleaved mica or mica pretreated by spermidine. All unadsorbed molecules were removed by buffer rinse and then by water [90]. To avoid dissociation of RNA associates, rinsing samples with water was performed quickly (<1 s). Experimental details for the use of the cryo-AFM instrumentation are described in [91,92].

AFM imaging of pRNA molecules [90] confirms that pRNA can form a variety of structures and shapes, including dimers, tetramers, rods, triangles, and 3D arrays via interaction of programmed helical regions and loops (Fig. 6). For example, the pRNA monomers folded into a checkmark shape 16.7 ± 0.9 nm long (Fig. 6A),

dimers displayed a rod shape 30.2 ± 2.5 nm long and 11.6 ± 1.4 nm wide (Fig. 6B), trimers exhibited a triangle shape 30.3 ± 2.4 nm on each side (Fig. 6C), and arrays displayed as bundles several microns in size (Fig. 6D) [35,90]. It should be noted that pRNA arrays form only in the presence of 1 M of monovalent ions such as NaCl, although the buffer already contains 5 mM of divalent ions, such as $MgCl_2$ or $CaCl_2$ [35,90]. Such arrays are more stable and resistant to the temperature, salt concentration, and pH than linear 120-nucleotide RNA. This is due to the tight folding in the pRNA structure and the intertwining of the RNA molecule in the arrays.

One of the limiting factors of cryo-AFM is that the sample must be imaged just after its preparation. Prolonged storage of a sample in the preparation box results in sample deterioration [92,93]. Note, however, that similar resolution has been achieved for analogous RNA designs recently [60]. One set of images from this paper is shown in Fig. 7. A good correlation between expected shapes for the constructs (plates A and B) and the AFM images (plates C–F) are seen. Note almost a coincidence between the model (plate B) and AFM images for this construct in plate F. The In this paper the images were obtained at room temperature using a regular AFM. The APS-mica sample preparation procedure was used in those experiments.

4. High-speed AFM imaging of DNA and its complexes

Conventional atomic force microscopes operate rather slowly. Typically, it takes at least 30–60 s to capture an image. Several groups developed designs with higher data acquisition speed. The first fast scanning AFM was made by the group of AFM co-inventor Quate [94]. This design integrated self-actuation cantilevers and used cantilever arrays to achieve high scanning speed. However, the stiffness of the active probes did not allow imaging
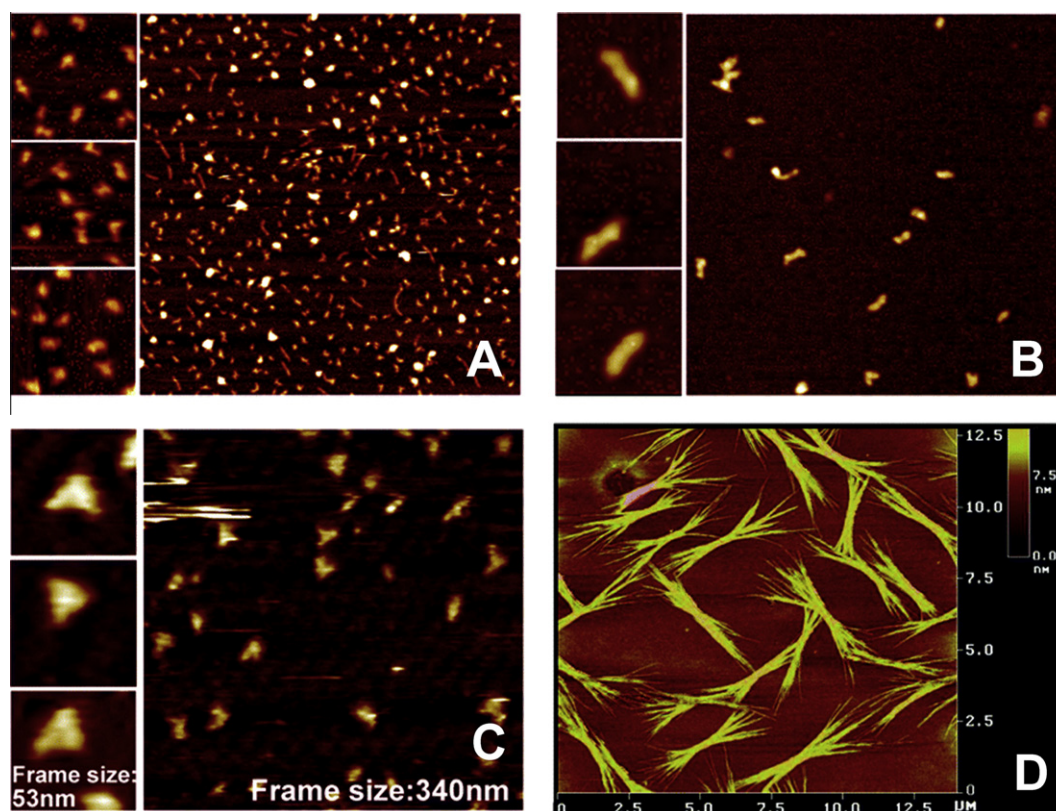

Fig. 6. Cryo-AFM images of pRNA monomers (A), dimers (B), trimers (C), and arrays (D). The frame sizes of images A and B are identical to the frame size of image C. The figure was reprinted from publication [90]; copyright © 2004 with permission of the American Chemical Society.
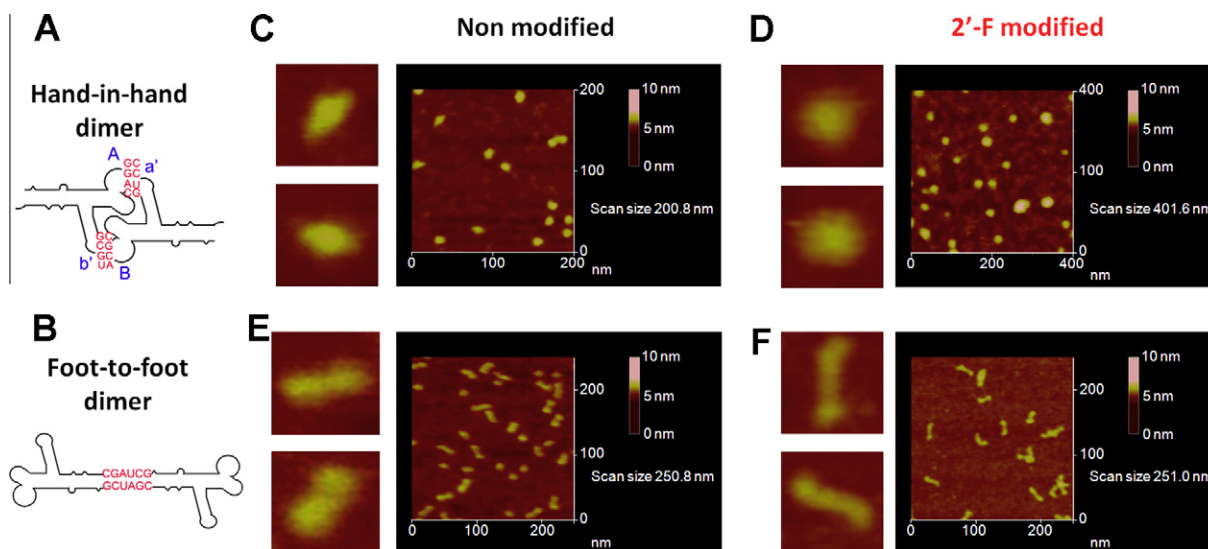
Fig. 7. Atomic force microscopy images showing hand-in-hand and foot-to-foot dimer nanoparticles of nonmodified pRNA and 2 = −FC/U pRNA, respectively. Plates A and B are the model for the constructs. Plates C–F are the AFM images for both constructs with zoomed images are shown to the left of the corresponding large scale images. The images were acquired in air with TM AFM (Veeco). APS-mica procedure was used for the preparation of samples. The figure was reprinted from publication [60]; copyright © with permission of the American Chemical Society.

of soft biological systems. A breakthrough in the development of a high-speed AFM (HS-AFM) for biological application was made after implementing the short cantilever idea proposed by Hansma [95]. The initial HS-AFM design of the Hansma group provided data acquisition at a rate of 0.5 frames/s, which was 100 times faster than the rate of a conventional AFM. T. Ando's group further developed the short cantilever idea by improving the design of the scanner and by developing the fast data acquisition electronics [96]. With this new design, the Ando team could acquire images in aqueous solution with a sub-second data acquisition rate and observe the dynamics of myosin at 12.5 frames/s for a 240-nm^2 area with 100 × 100 pixel resolution. Later improvements led to an instrument operating at video rate [96–98], and its implementation in other labs made it possible to observe molecular dynamics on a millisecond time scale [99–103]. The sections below describe the overview and performance of the instrument and the data on imaging segmental dynamics of DNA.

4.1. Overview of tapping-mode HS-AFM

A scheme of the HS-AFM setup is depicted in Fig. 8. The optical method is used to measure deflection of the cantilever (3). The optical beam deflection (OBD) detector was developed according to the idea of Schaffer et al. [104,105]. Cantilevers for fast imaging are approximately 10-times smaller than conventional ones (i.e., 6–10 μm long, 2 μm wide, and 90 nm thick), and the resonant frequency and the spring constant are 600 kHz-1.2 MHz in water and 0.1–0.2 N/m, respectively [106]. Small cantilevers with a resonant frequency of ∼600 kHz in water are now commercially available (AC-10; Olympus, Tokyo, Japan). Because of the small size of high-speed cantilevers, the optics of the OBD detector must generate a very small incident beam spot. The objective lenses (Fig. 8, labeled 9) focus the laser spot on the rear side of the cantilever (3); the reflected laser beam is collected and collimated with the same objective lenses (9). The incident and reflected light beams are separated using a polarization beam splitter (12) and a quarter-wave plate (11). Then, they are reflected onto the split photodiode (15). The cantilever (3) is attached to a transparent glass plate via a short cantilever holder glued to the glass plate. The rear side of the cantilever faces downward and the tip faces upward. The scanner (1) with a sample stage (2) is mounted facing downward,

so the specimen is supported at the bottom of the sample stage and inverted to the level of the cantilever probe. The angle between the tip and the sample is achieved by the angular position of the scanner with a sample stage.

Three key factors provide the high-speed imaging capability of the instrument [97,98]: (i) high bandwidth of the feedback control to maintain the tip–sample distance, (ii) active damping to suppress the scanner's mechanical vibrations, and (iii) low-invasive techniques to minimize the tip–sample interaction force. To achieve the fast feedback operation, almost all devices of AFM are optimized for fast response. For more comprehensive descriptions of HS-AFM techniques, see paper [98]. An older version of the HS-AFM apparatus is commercially available only in Japan, but the most recent version is not yet available. We expect that it will be commercially available world-wide within 2 years.

4.2. Performance of HS-AFM

The highest possible imaging rate of the most recent version of the HS-AFM has reached ∼25 frames/s at a 250 × 250 nm^2 scan range, 100 scan lines, and 0.1/nm spatial frequency of sample topography. Importantly, this high imaging rate is compatible with low-invasive imaging. That is, the tip–sample interaction does not disturb weak protein–protein and protein–DNA interactions. The mechanical quantity that affects the sample is not the force itself but the force impulse, i.e., the product of force and the time over which the force acts. In tapping-mode HS-AFM, the duration of the force action is short (∼100 ns), and therefore, a relatively large peak force (∼30 pN) would not affect the sample significantly.

At a high imaging rate, the sample stage is moved quickly in the z-direction to maintain the cantilever oscillation amplitude (and hence the tip–sample interaction force) constant. This quick displacement generates a large hydrodynamic pressure, which could affect the sample as well as the dynamics of cantilever oscillation. The effects from this hydrodynamic pressure become negligible by the following means: First, a small sample stage ∼2 mm in diameter is used [107]. Second, the cantilever tip is placed at an edge region of the small sample stage so that the whole cantilever chip is minimally overlapped with the sample stage. Third, the tip length is adjusted to longer than ∼2.5 μm.
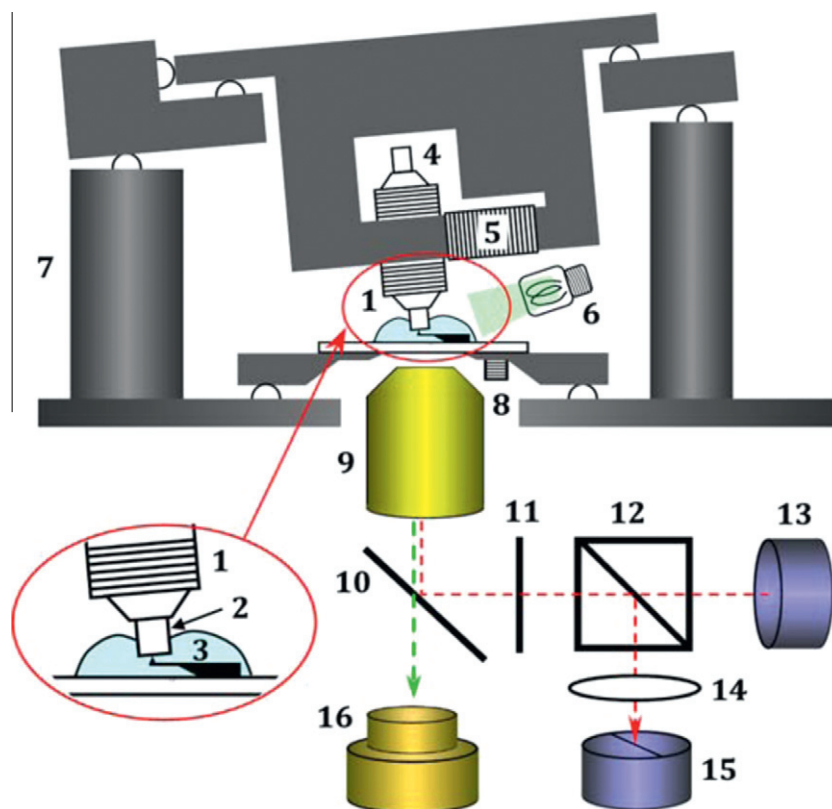
Fig. 8. Schematic drawing of the HS-AFM head integrated with an inverted type of optical microscope. Z-piezo scanner (1), sample stage (2), cantilever (3), counter weight (4), x-piezo scanner (5), illuminator (6), stepper motor (7), piezo for exciting cantilever (8), objective lens (9), dichroic mirror (10), quarter wave plate (11), polarization beam splitter (12), laser diode (13), focusing lens (14), split photodiode (15), and CCD camera (16).

The above-mentioned capabilities of HS-AFM have made it possible to directly visualize dynamic processes involving protein and nucleic acid molecules in millisecond time scales [96,98,108,109]. For example, the dynamic behavior of myosin V molecules walking along actin filaments was successfully captured on video [109]. For this observation, partially biotinylated actin filaments were immobilized onto a planar lipid bilayer surface containing a biotin–lipid, and myosin V molecules were nearly free on the surface. The walking velocity detected therein was very similar to that measured by fluorescence microscopy, indicating negligible effects of the tip–sample and surface–sample interactions. The molecular movies simultaneously showed known and unknown behaviors of functioning myosin V, leading to a comprehensive understanding of its motor mechanism. Another example is the time-lapse imaging of bacteriorhodopsin (bR) dynamics within native purple membranes. The proteins dynamically change their structure in response to light stimuli. Upon light illumination, part of each bR molecule is displaced outward from the trimer center. As a result, three nearest-neighbor bR monomers, each of which belongs to a different adjacent trimer, are brought into contact with each other. This transient bR–bR interaction elicits both positive and negative cooperative effects on the decay kinetics as the initial bR recovers.

4.3. Imaging of DNA segmental dynamics with HS-AFM

Successful imaging of DNA dynamics or the dynamics of other biological systems requires the ability of the system to move over the AFM substrate. At the same time, the sample should remain bound within the scanning area during imaging. Selection of an appropriate sample preparation procedure can accommodate these conflicting conditions. For example, the cation-assisted methodology with Mg^{2+} was used [100] to observe the dynamics of DNA in

complexes with the EcoP151 restriction enzyme. This study observed ATP-dependent translocation of the enzyme. A similar immobilization technique was applied in [101] to image the interaction of biotinylated DNA with streptavidin. Similar approach with the use of Ca^{2+} was applied to image the interaction of EcoRII restriction enzyme with DNA [102]. The use of HS AFM made it possible to directly image various pathways of the search mechanism employed by this protein. In a recent study [103], mica was modified by spermidine before sample deposition. With this modification, negatively charged biological molecules can be directly adsorbed onto the positively charged mica surface without adding cations. The specifics for each sample preparation procedure can be found in the papers cited above. We will specify some general features of the methods. The solution, containing the biological sample (2 μl), is deposited onto the surface of freshly cleaved mica (1–2 mm in diameter) for 1–15 min. After that, the sample is rinsed with buffer to remove unattached molecules; it is then scanned in the imaging buffer without a drying step. Generally, the rinsing and imaging buffers are the same.

To illustrate the power of the fast scanning AFM for studies of nucleic acids, we briefly describe the results of imaging the segmental dynamics of DNA. A solution (2 μl) of the DNA fragment (491 bp, 167 nm) in 10 mM HEPES buffer containing 5 mM Mg^{2+} cations was placed on the surface of freshly cleaved mica, left for 2 min, rinsed with the same buffer, and imaged with an HS-AFM instrument (RIBM Co., Ltd.). The data acquisition rate was three frames per second. One frame is shown in Fig. 9A. The shape of the DNA molecule is consistent with images obtained with traditional AFM, and the curvy morphology reflects DNA flexibility. The DNA paths on this and other images were traced and superimposed by aligning the top left ends of the molecules. Fig. 9B–D show the superimposing of 20, 40 and 60 frames, respectively.
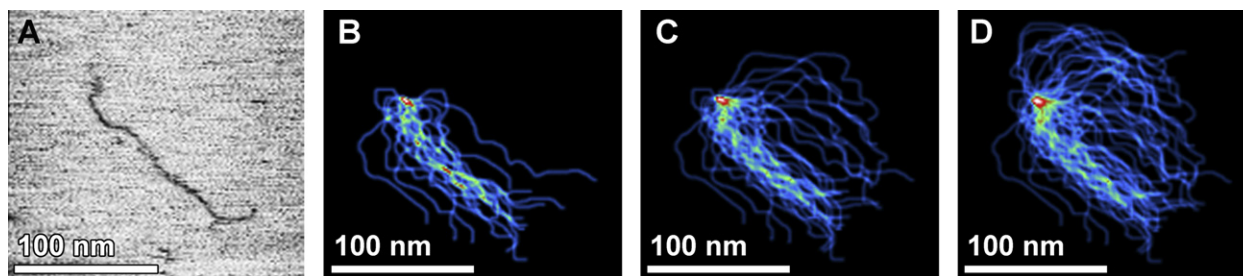
Fig. 9. (A) Single frame of an HS-AFM image obtained at three frames per second. DNA strands were traced in successive frames and the traced images were overlaid. (B) 20 frames; (C) 40 frames; (D) 60 frames.

These data demonstrate that over time, DNA undergoes substantial segmental motion that leads to a change in the entire morphology of the molecule.

Time-lapse imaging is the most attractive mode of AFM, as the dynamics of biological systems can be observed with nanometer spatial resolution. The critical issue with this mode is its potential tip dragging effect due to the inevitable tip–sample interaction. Tapping mode decreases this effect because the tip is in contact with the sample for only a short time. The tip–sample interaction is further decreased by the drive amplitude of the tip oscillation, as the energy that the tip transmits to the sample depends quadratically on this parameter [63]. The drive amplitude issue is especially important for HS-AFM due to its elevated scanning speed. Therefore, this instrument was designed to operate at low drive amplitude since it operates with amplitudes an order of magnitude lower than traditional AFM. To investigate a potential dragging effect [101], the movement rates of DNA segments along the tip scanning direction and perpendicular to the HS-AFM instrument were analyzed. A difference between scanning directions has not been found, suggesting that the lateral force applied to the sample does not increase with increasing scan rate. Additional studies recently analyzed the elastic bending energies and fluctuations of single-molecule conformations induced by the AFM probe [103]. The findings demonstrate that the AFM tip does not contribute to the whole value of DNA thermal energy and the drag effects are negligible.

5. Conclusions

AFM has emerged from the development stage and is currently being applied to various molecular biology problems, which often require direct imaging of nucleic acids. Among the various imaging modes of AFM, time-lapse nanoimaging is the most attractive, as biological processes can be imaged at nanometer resolution. Instrument development combined with advances in the sample preparation techniques has made it possible to study the molecular mechanisms of such processes as homologous DNA recombination and chromatin dynamics. Moreover, the instrumentation and the necessary methodology for high-speed AFM have already passed the development stage. As a result, an instrument capable of imaging the dynamics of molecules at video rate has become available to the biomedical community. Currently, several groups have applied the technology to the most critical biological problems and have already made a number of important discoveries including those in RNA nanotechnology.

Acknowledgments

References

[1] N.C. Seeman, Mol. Biotechnol. 37 (2007) 246–257.
[2] P. Guo, Nat. Nanotechnol. 5 (2010) 833–842.
[3] P. Guo, J. Nanosci. Nanotechnol. 5 (2005) 1964–1982.
[4] P. Guo, O. Coban, N.M. Snead, J. Trebley, S. Hoeprich, S. Guo, Y. Shu, Adv. Drug Deliv. Rev. 62 (2010) 650–666.
[5] C. Bustamante, J. Vesenka, C.L. Tang, W. Rees, M. Guthold, R. Keller, Biochemistry 31 (1992) 22–26.
[6] Y.L. Lyubchenko, B.L. Jacobs, S.M. Lindsay, Nucleic Acids Res. 20 (1992) 3983–3986.
[7] J. Yang, K. Takeyasu, Z. Shao, FEBS Lett. 301 (1992) 173–176.
[8] J. Vesenka, M. Guthold, C.L. Tang, D. Keller, E. Delaine, C. Bustamante, Ultramicroscopy 42–44 (Pt B) (1992) 1243–1249.
[9] M.J. Allen, X.F. Dong, T.E. O'Neill, P. Yau, S.C. Kowalczykowski, J. Gatewood, R. Balhorn, E.M. Bradbury, Biochemistry 32 (1993) 8390–8396.
[10] C. Bustamante, D.A. Erie, D. Keller, Curr. Opin. Struct. Biol. 4 (1994) 750–760.
[11] J. Mou, D.M. Czajkowsky, Y. Zhang, Z. Shao, FEBS Lett 371 (1995) 279–282.
[12] C. Bustamante, C. Rivetti, D.J. Keller, Curr. Opin. Struct. Biol. 7 (1997) 709–716.
[13] Y.L. Lyubchenko, A.A. Gall, L.S. Shlyakhtenko, Methods Mol. Biol. 148 (2001) 569–578.
[14] Y.L. Lyubchenko, A.A. Gall, L.S. Shlyakhtenko, R.E. Harrington, B.L. Jacobs, P.I. Oden, S.M. Lindsay, J. Biomol. Struct. Dyn. 10 (1992) 589–606.
[15] Y.L. Lyubchenko, L.S. Shlyakhtenko, T. Aki, S. Adhya, Nucleic Acids Res. 25 (1997) 873–876.
[16] C. Bustamante, M. Guthold, X. Zhu, G. Yang, J. Biol. Chem. 274 (1999) 16665–16668.
[17] L.S. Shlyakhtenko, A.A. Gall, A. Filonov, Z. Cerovac, A. Lushnikov, Y.L. Lyubchenko, Ultramicroscopy 97 (2003) 279–287.
[18] R.W. Keller, D.J. Keller, D. Bear, J. Vasenka, C. Bustamante, Ultramicroscopy 42–44 (Pt B) (1992) 1173–1180.
[19] M. Hegner, P. Wagner, G. Semenza, FEBS Lett. 336 (1993) 452–456.
[20] P. Wagner, P. Kernen, M. Hegner, E. Ungewickell, G. Semenza, FEBS Lett. 356 (1994) 267–271.
[21] P. Wagner, M. Hegner, P. Kernen, F. Zaugg, G. Semenza, Biophys. J. 70 (1996) 2052–2066.
[22] O. Medalia, J. Englander, R. Guckenberger, J. Sperling, Ultramicroscopy 90 (2002) 103–112.
[23] S. Yonghai, L. Zhuang, L. Zhiguo, W. Gang, W. Li, S. Lanlan, Microsc. Res. Tech. 68 (2005) 59–64.
[24] A. Ikai, Surf. Sci. Rep. 26 (1996) 261–332.
[25] T.-W. Wang, H.-Y. Lu, P.-J. Lou, F.-H. Lin, Biomaterials 29 (2008) 4447–4454.
[26] E.I. Goksu, J.M. Vanegas, C.D. Blanchette, W.C. Lin, M.L. Longo, Biochim. Biophys. Acta 1788 (2009) 254–266.
[27] X. Jiang, X. Lin, Electrochem. Commun. 6 (2004) 873–879.
[28] A.M. Oliveira Brett, A.-M. Chiorcea Paquim, Bioelectrochemistry 66 (2005) 117–124.
[29] C. Spagnoli, A. Korniakov, A. Ulman, E.A. Balazs, Y.L. Lyubchenko, M.K. Cowman, Carbohydr. Res. 340 (2005) 929–941.
[30] J. Adamcik, D.V. Klinov, G. Witz, S.K. Sekatskii, G. Dietler, FEBS Lett. 580 (2006) 5671–5675.
[31] E.V. Dubrovin, J.W. Gerritsen, J. Zivkovic, I.V. Yaminsky, S. Speller, Colloids Surf. B 76 (2010) 63–69.
[32] Y.L. Lyubchenko, L.S. Shlyakhtenko, Methods 47 (2009) 206–213.
[33] Y.L. Lyubchenko, L.S. Shlyakhtenko, A.A. Gall, Methods Mol. Biol. 543 (2009) 337–351.
[34] N.C. Seeman, Methods Mol. Biol. 303 (2005) 143–166.

[35] C. Chen, S. Sheng, Z. Shao, P. Guo, J. Biol. Chem. 275 (2000) 17510–17516.
[36] Z. Liu, Z. Li, H. Zhou, G. Wei, Y. Song, L. Wang, Micron 36 (2005) 525–531.
[37] H.G. Hansma, D.E. Laney, Biophys. J. 70 (1996) 1933–1939.
[38] N.H. Thomson, S. Kasas, Smith, H.G. Hansma, P.K. Hansma, Langmuir 12 (1996) 5905–5908.
[39] P.R. Dahlgren, Y.L. Lyubchenko, Biochemistry 41 (2002) 11372–11378.
[40] J. Zheng, Z. Li, A. Wu, H. Zhou, Biophys. Chem. 104 (2003) 37–43.
[41] F. Kienberger, L.T. Costa, R. Zhu, G. Kada, M. Reithmayer, L. Chtcheglova, C. Rankl, A.B. Pacheco, S. Thalhammer, V. Pastushenko, W.M. Heckl, D. Blaas, P. Hinterdorfer, Biomaterials 28 (2007) 2403–2411.
[42] K. Zhang, H. Qi, H. Li, Y. Liu, W. Chen, Scanning 31 (2009) 75–82.
[43] H.G. Hansma, R. Golan, W. Hsieh, C.P. Lollo, P. Mullen-Ley, D. Kwoh, Nucleic Acids Res. 26 (1998) 2481–2487.
[44] C. Brack, CRC Crit. Rev. Biochem. 10 (1981) 113–169.
[45] T. Thundat, D.P. Allison, R.J. Warmack, G.M. Brown, K.B. Jacobson, J.J. Schrick, T.L. Ferrell, Scanning Microsc. 6 (1992) 911–918.
[46] H.G. Hansma, M. Bezanilla, F. Zenhausern, M. Adrian, R.L. Sinsheimer, Nucleic Acids Res. 21 (1993) 505–512.
[47] M. Bezanilla, M. Srinivas, D.E. Laney, Y.L. Lyubchenko, H.G. Hansma, Adsorption of DNA to Mica Silylated mica and Minerals: Characterization by Atomic Force Microscopy, American Chemical Society, Washington, DC, ETATS-UNIS, 1995.
[48] D. Pastre, O. Pietrement, S. Fusil, F. Landousy, J. Jeusset, M.O. David, L. Hamon, E. Le Cam, A. Zozime, Biophys. J. 85 (2003) 2507–2518.
[49] F.J. Solis, J. Chem. Phys. 117 (2002) 9009–9015.
[50] R. Das, T.T. Mills, L.W. Kwok, G.S. Maskel, I.S. Millett, S. Doniach, K.D. Finkelstein, D. Herschlag, L. Pollack, Phys. Rev. Lett. 90 (2003) 188103.
[51] H. Cheng, K. Zhang, J.A. Libera, M. Olvera de la Cruz, M.J. Bedzyk, Biophys. J. 90 (2006) 1164–1174.
[52] P. Kekicheff, S. Marcelja, T.J. Senden, V.E. Shubin, J. Chem. Phys. 99 (1993) 6098–6113.
[53] W. Han, M. Dlakic, Y.J. Zhu, S.M. Lindsay, R.E. Harrington, Proc. Natl. Acad. Sci. USA 94 (1997) 10565–10570.
[54] W. Han, S.M. Lindsay, M. Dlakic, R.E. Harrington, Nature 386 (1997) 563.
[55] P.A. Wiggins, T. van der Heijden, F. Moreno-Herrero, A. Spakowitz, R. Phillips, J. Widom, C. Dekker, P.C. Nelson, Nat. Nanotechnol. 1 (2006) 137–141.
[56] G. Zuccheri, B. Samori, Methods Cell Biol. 68 (2002) 357–395.
[57] A. Vologodskii, N.R. Cozzarelli, Biophys. J. 70 (1996) 2548–2556.
[58] D.I. Cherny, T.M. Jovin, J. Mol. Biol. 313 (2001) 295–307.
[59] Y.L. Lyubchenko, R.E. Blankenship, A.A. Gall, S.M. Lindsay, O. Thiemann, L. Simpson, L.S. Shlyakhtenko, Scanning Microsc. Suppl. 10 (1996) 97–107 (discussion 07–09).
[60] J. Liu, S. Guo, M. Cinier, L.S. Shlyakhtenko, Y. Shu, Chaoping Chen, G. Shen, P. Guo, ACS Nano, in press, doi:10.1021/nn1024658.
[61] S.M. Lindsay, N.J. Tao, J.A. DeRose, P.I. Oden, L. Lyubchenko Yu, R.E. Harrington, L. Shlyakhtenko, Biophys. J. 61 (1992) 1570–1584.
[62] L.S. Shlyakhtenko, L. Miloseska, V.N. Potaman, R.R. Sinden, Y.L. Lyubchenko, Ultramicroscopy 97 (2003) 263–270.
[63] Y.L. Lyubchenko, L.S. Shlyakhtenko, Proc. Natl. Acad. Sci. USA 94 (1997) 496–501.
[64] S. Hsieh, W.-J. Chao, C.-W. Hsieh, J. Nanosci. Nanotechnol. 9 (2009) 2894–2901.
[65] Z. Shao, J. Mou, D.M. Czajkowsky, J. Yang, J.-Y. Yuan, Adv. Phys. 45 (1996) 1–86.
[66] T.W. Jing, A.M. Jeffrey, J.A. DeRose, Y.L. Lyubchenko, L.S. Shlyakhtenko, R.E. Harrington, E. Appella, J. Larsen, A. Vaught, D. Rekesh, et al., Proc. Natl. Acad. Sci. USA 90 (1993) 8934–8938.
[67] D. Rekesh, Y. Lyubchenko, L.S. Shlyakhtenko, S.M. Lindsay, Biophys. J. 71 (1996) 1079–1086.
[68] T. Ohshiro, M. Maeda, Chem. Commun. (Camb). 46 (2010) 2581–2583.
[69] E. Shapir, H. Cohen, N. Borovok, A.B. Kotlyar, D. Porath, J. Phys. Chem. B 110 (2006) 4430–4433.
[70] T.P. Beebe Jr., T.E. Wilson, D.F. Ogletree, J.E. Katz, R. Balhorn, M.B. Salmeron, W.J. Siekhaus, Science 243 (1989) 370–372.
[71] P.G. Arscott, G. Lee, V.A. Bloomfield, D.F. Evans, Nature 339 (1989) 484–486.
[72] G. Lee, P.G. Arscott, V.A. Bloomfield, D.F. Evans, Science 244 (1989) 475–477.
[73] C.R. Clemmer, T.P. Beebe Jr., Science 251 (1991) 640–642.
[74] Y.L. Lyubchenko, S.M. Lindsay, J.A. DeRose, T. Thundat, J. Vac. Sci. Technol. B 9 (1991) 1288–1290.
[75] D. Klinov, B. Dwir, E. Kapon, N. Borovok, T. Molotsky, A. Kotlyar, Nanotechnology 18 (2007) 225102.
[76] J. Adamcik, S. Tobenas, G. Di Santo, D. Klinov, G. Dietler, Langmuir 25 (2009) 3159–3162.
[77] Q. Zhong, D. Inniss, K. Kjoller, V.B. Elings, Surf. Sci. Lett. 290 (1993) L688–L692.
[78] P. Guo, Nat Nanotechnol 5 (2010) 833–842.
[79] E.A. Oussatcheva, L.S. Shlyakhtenko, R. Glass, R.R. Sinden, Y.L. Lyubchenko, V.N. Potaman, J. Mol. Biol. 292 (1999) 75–86.
[80] L.S. Shlyakhtenko, V.N. Potaman, R.R. Sinden, A.A. Gall, Y.L. Lyubchenko, Nucleic Acids Res. 28 (2000) 3472–3477.
[81] L.S. Shlyakhtenko, D. Rekesh, S.M. Lindsay, I. Kutyavin, E. Appella, R.E. Harrington, Y.L. Lyubchenko, J. Biomol. Struct. Dyn. 11 (1994) 1175–1189.
[82] L.S. Shlyakhtenko, E. Appella, R.E. Harrington, I. Kutyavin, Y.L. Lyubchenko, J. Biomol. Struct. Dyn. 12 (1994) 131–143.
[83] R. Holliday, Genetics Res. 5 (1964) 282–304.
[84] D.M. Lilley, Q. Rev. Biophys. 41 (2008) 1–39.
[85] A.Y. Lushnikov, A. Bogdanov, Y.L. Lyubchenko, J. Biol. Chem. 278 (2003) 43130–43134.
[86] N.C. Seeman, Trends Biochem. Sci. 30 (2005) 119–125.
[87] H.G. Hansma, E. Oroudjev, S. Baudrey, L. Jaeger, J. Microsc. 212 (2003) 273–279.
[88] A. Chworos, I. Severcan, A.Y. Koyfman, P. Weinkam, E. Oroudjev, H.G. Hansma, L. Jaeger, Science 306 (2004) 2068–2072.
[89] P. Guo, C. Zhang, C. Chen, K. Garver, M. Trottier, Mol. Cell 2 (1998) 149–155.
[90] D. Shu, W.-D. Moll, Z. Deng, C. Mao, P. Guo, Nano Lett. 4 (2004) 1717–1723.
[91] S. Sheng, Z. Shao, Methods Cell Biol. 68 (2002) 243–256.
[92] Y. Zhang, S. Sheng, Z. Shao, Biophys. J. 71 (1996) 2168–2176.
[93] Y. Zhang, Z. Shao, A.P. Somlyo, A.V. Somlyo, Biophys. J. 72 (1997) 1308–1318.
[94] S.R. Manalis, S.C. Minne, A.C.F. Quate, Appl. Phys. Lett. 68 (1996) 871–873.
[95] D.A. Walters, J.P. Cleveland, N.H. Thomson, P.K. Hansma, M.A. Wendman, G. Gurley, V. Elings, Rev. Sci. Instrum. 67 (1996) 3583–3590.
[96] T. Ando, N. Kodera, E. Takai, D. Maruyama, K. Saito, A. Toda, Proc. Natl. Acad. Sci. USA 98 (2001) 12468–12472.
[97] T. Ando, T. Uchihashi, N. Kodera, D. Yamamoto, M. Taniguchi, A. Miyagi, H. Yamashita, J. Mol. Recognit. 20 (2007) 448–458.
[98] T. Ando, T. Uchihashi, T. Fukuma, Prog. Surf. Sci. 83 (2008) 337–437.
[99] Q. Zou, K. Leang, E. Sadoun, M. Reed, S. Devasia, Asian J. Control 6 (2004) 164–178.
[100] N. Crampton, M. Yokokawa, D.T. Dryden, J.M. Edwardson, D.N. Rao, K. Takeyasu, S.H. Yoshimura, R.M. Henderson, Proc. Natl. Acad. Sci. USA 104 (2007) 12755–12760.
[101] M. Kobayashi, K. Sumitomo, K. Torimitsu, Ultramicroscopy 107 (2007) 184–190.
[102] J.L. Gilmore, Y. Suzuki, G. Tamulaitis, V. Siksnys, K. Takeyasu, Y.L. Lyubchenko, Biochemistry 48 (2009) 10492–10498.
[103] Y. Suzuki, Y. Higuchi, K. Hizume, M. Yokokawa, S.H. Yoshimura, K. Yoshikawa, K. Takeyasu, Ultramicroscopy 110 (2010) 682–688.
[104] T.E. Schaffer, J.P. Cleveland, F. Ohnesorge, D.A. Walters, P.K. Hansma, J. Appl. Phys. 80 (1996) 3622–3627.
[105] T.E. Schaffer, P.K. Hansma, J. Appl. Phys. 84 (1998) 4661–4666.
[106] M. Kitazawa, K. Shiotani, A. Toda, Jpn. J. Appl. Phys. 42 (2003) 4844–4847.
[107] T. Ando, N. Kodera, D. Maruyama, E. Takai, K. Saito, A. Toda, Jpn. J. Appl. Phys. 41 (2002) 4851.
[108] M. Shibata, H. Yamashita, T. Uchihashi, H. Kandori, T. Ando, Nat. Nanotechnol. 5 (2010) 208–212.
[109] N. Kodera, D. Yamamoto, R. Ishikawa, T. Ando, Nature 468 (2010) 72–76.